Received 28 March 2025
Revised 11 May 2025
Accepted 13 May 2025

Study on the optimal test parameters for vibration compaction based on the control of physical-mechanical indicators

Zhongrui Chen, Yanxi Xiong and Ronghui Yan
School of Intelligent Manufacturing and Smart Transportation, Suzhou City University, Suzhou, China
Zhibo Cheng
Institute of Computing Technologies, China Academy of Railway Sciences Corporation Limited, Beijing, China
Taifeng Li
Railway Engineering Research Institute, China Academy of Railway Sciences Corporation Limited, Beijing, China, and
Hongfu Tan
National Railway Administration Engineering Quality Supervision Center, Beijing, China

Abstract

Purpose – The indoor vibration compaction test (*IVCT*) was a key step in controlling the compaction quality for high-speed railway graded aggregate (*HRGA*), which currently had a research gap on the assessment indicators and compaction parameters.

Design/methodology/approach – To address these issues, a novel multi-indicator *IVCT* method was proposed, including physical indicator dry density (ρ_d) and mechanical indicators dynamic stiffness (K_{rb}) and bearing capacity coefficient (K_{20}). Then, a series of *IVCT*s on *HRGA* under different compaction parameters were conducted with an improved vibration compactor, which could monitor the physical-mechanical indicators in real-time. Finally, the optimal vibration compaction parameters, including the moisture content (ω), the diameter-to-maximum particle size ratio (R_d), the thickness-to-maximum particle size ratio (R_h), the vibration frequency (f), the vibration mass (M_c) and the eccentric distance (r_e), were determined based on the evolution characteristics for the physical-mechanical indicators during compaction.

Findings – All results indicated that the ρ_d gradually increased and then stabilized, and the K_{rb} initially increased and then decreased. Moreover, the inflection time of the K_{rb} was present as the optimal compaction time (T_{lp}) during compaction. Additionally, optimal compaction was achieved when ω was the water-holding content after mud pumping, R_d was 3.4, R_h was 3.5, f was the resonance frequency, and the ratio between the excitation force and the M_c was 1.8.

Originality/value – The findings of this paper were significant for the quality control of *HRGA* compaction.

Keywords High-speed railway subgrade, Graded aggregates, Vibratory compaction test, Optimal vibration compaction parameters, Physical-mechanical indicator

Paper type Research paper

This research was funded by the National Key R&D Program "Transportation Infrastructure" project (No. 2022YFB2603400), the Technology Research and Development Plan Program of China State Railway Group Co., Ltd. (No. Q2024T001) and the National project pre research project of Suzhou City University (No. 2023SGY019).

Railway Sciences
Vol. 4 No. 3, 2025
pp. 388-409
Emerald Publishing Limited
e-ISSN: 2755-0915
p-ISSN: 2755-0907
DOI 10.1108/RS-03-2025-0007

1. Introduction

The high-speed railway subgrade served as the foundation that bears both the static load of the rail structure and the dynamic load from train operations (Lan *et al.*, 2023; Wu, Fu, & Bian, 2024). It primarily consisted of high-speed railway graded aggregate (*HRGA*) with desirable physical-mechanical properties (Xiao *et al.*, 2023; Xie *et al.*, 2023a, b). To ensure the stability and durability of the subgrade and maintain its service performance, strict control over the compaction quality of *HRGA* fillers was essential. Inadequate compaction quality control could lead to subgrade defects, such as differential settlement (Ye *et al.*, 2021a), mud pumping (Indraratna & Nguyen, 2021; Chawla & Shahu, 2016) and track shift (Yang, Yue, & Tai, 2021), which were detrimental to the safety of high-speed railway operations.

The compaction degree (K) was the key indicator to assess the compaction quality of the subgrade, which was the ratio of the field dry density (ρ_{df}) to the maximum dry density (ρ_{dmax}) obtained from the indoor compaction test (Yong *et al.*, 2022). The ρ_{df} was obtained using the sand cone method, which proved to be a reasonable and accurate approach. The ρ_{dmax} could be measured either through indoor heavy hammer compaction tests or indoor vibration compaction tests (IVCTs) (Chen, Xie, & Li, 2023). Previous studies showed that *IVCT* increased ρ_{dmax} for *HRGA* by 2% to 5% and improved its mechanical properties by 20% to 40% compared to the heavy hammer compaction approach (Xie *et al.*, 2023a, b; Spagnoli & Shimobe, 2020; Sarsam & Jumaah, 2016). It was currently recognized as a compaction approach that closely resembled the roller compaction in the field, widely applied in hydraulic and highway construction. Moreover, it was also the test method for determining the maximum dry density of gravel fillers as required by the *code for soil test of railway engineering (TB 10102–2010)* (China Railway First Survey and Design Institute Group Corporation Limited, 2010). Hence, *IVCT* was a critical step in controlling the compaction quality of *HRGA*. However, the compaction equipment, methods and parameters were primarily designed for materials such as inorganic binders (asphalt) used in highways and coarse-grained soils used in hydraulic dams, which were not suitable for *HRGA* fillers. This significantly impeded the widespread application of *IVCT* in railway subgrade construction.

In recent years, extensive research on *IVCT* was conducted, primarily focusing on compaction equipment and parameters (Wang *et al.*, 2024; Dan, Yang, & Liu, 2020). For example, novel indoor vibration compaction equipment was developed by Xie *et al.* (2023), significantly improving testing efficiency and standardization. Furthermore, two particle motion indicators significantly related to compaction quality were proposed through *IVCT* by Xiao *et al.* (2024b), and the effects of gradation and frequency on the vibration compaction quality of coarse-grained soils were investigated. Moreover, a machine learning prediction model for the optimal moisture content of coarse-grained soils was proposed by Xie *et al.* (2023a, b) based on extensive *IVCT*. It was clearly observed that existing research mainly focused on the impact of coarse-grained soil parameters on compaction quality, with a lack of studies on the optimal parameters for vibration compaction equipment (e.g. frequency, equipment size, etc.). Hence, it was necessary to conduct research on the optimal parameters for vibration compaction equipment to improve the standardization and accuracy of *IVCT*.

In summary, to determine optimal vibration compaction parameters for graded aggregates in *IVCT*, this study proposed a multi-indicator evaluation method for compaction quality control, incorporating dry density (ρ_d), dynamic stiffness (K_{rb}) and bearing capacity coefficient (K_{20}). Then, extensive vibration compaction tests were conducted to determine the optimal vibration compaction parameters for graded aggregates. Finally, a standardized method for determining the optimal parameters was proposed. The findings contributed to enhancing the quality control of graded aggregate compaction.

2. Novel indoor vibration compaction test

2.1 Traditional vibration compaction test

The compaction degree (K) was the key indicator to assess the compaction quality for HRGA in the field, which could be calculated by Eq. (1) (Research Institute of Highway Ministry of Transport, 2019). It was key for calculating the K to determine the maximum dry density (ρ_d). Moreover, it was well known that the traditional IVCT was used to determine the maximum ρ_d for *HRGA* (Yong *et al.*, 2022), which could simulate vibration compaction in the field. Therefore, the *IVCT* was a key step in the compaction quality control for *HRGA*.

$$K = \frac{\rho_{df}}{\rho_{d\max}} \tag{1}$$

where ρ_{df} is the ρ_d measured in the field, $\rho_{d\max}$ is the maximum ρ_d measured in *IVCT*.

Nevertheless, the evolution characteristics of the ρ_d were one-sided and used to assess the compaction quality in the traditional *IVCT*, which lacked stiffness and strength indicators, as shown in Figure 1. Moreover, the compaction parameters were uncertain, which led to differences in *IVCT* results between projects, including the moisture content (ω), the diameter-to-maximum particle size ratio (R_d), the thickness-to-maximum particle size ratio (R_h), the vibration frequency (f), the vibration mass (M_c) and the eccentric distance (r_e). Applying traditional *IVCT* could lead to inadequate compaction quality control for *HRGA*. Hence, it was necessary to determine the optimal compaction parameters in the *IVCT* through systematic analysis, further improving the compaction quality control for *HRGA*.

2.2 Novel IVCT method

A novel *IVCT* method based on physical-mechanical indicators including physical indicator ρ_d and mechanical indicators dynamic stiffness (K_{rb}) and bearing coefficient (K_{20}) was proposed, which could assess the compaction quality for *HRGA*. The evolution characteristics for the indicators during compaction could be used to determine the optimal compaction parameters for *IVCT*, as shown in Figure 2.

2.2.1 Novel indicators. A continuous ρ_d test method was proposed, based on maintaining the constant mass of the *HRGA* filler during compaction and measuring the resulting volume

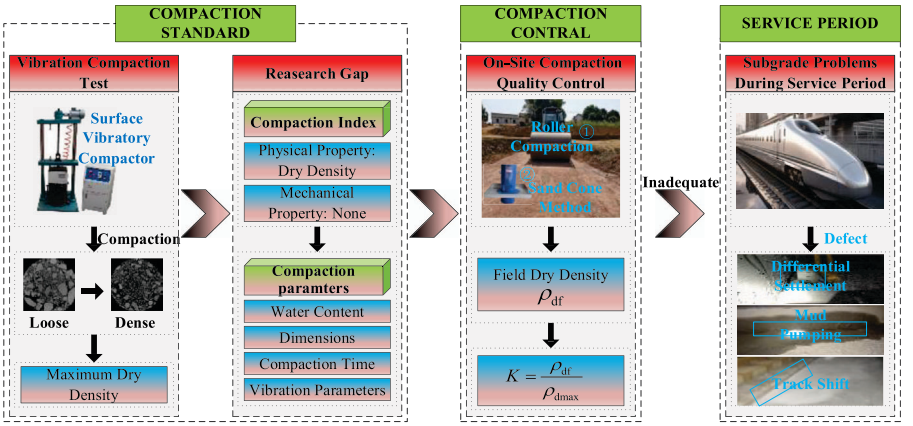

Figure 1. The research gap of traditional IVCT. **Source(s):** Authors' own work

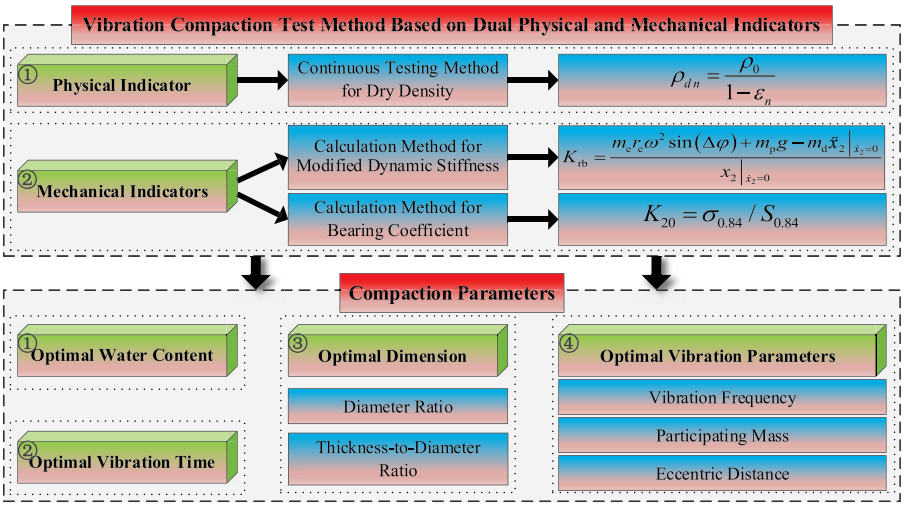

Figure 2. Novel IVCT method. **Source(s):** Authors' own work

change. The volume change resulted from the surface settlement of the *HRGA* filler during compaction, according to the previous research (Ye, Chen, & Hui, 2021b; Wang, Yu, & Xiao, 2022), the continuous ρ_d could be calculated as follows:

$$\rho_{dn}=\frac{mg}{A(h_0-S_n)} \tag{2}$$

where ρ_{dn} is the dry density of the *HRGA* filler after compaction n times, m is the *HRGA* filler mass, A is the container bottom area, h_0 is the initial height of the *HRGA* filler and S_n is the surface settlement of the *HRGA* filler after compaction n times.

However, ρ_{dn} only characterized the physical properties of the *HRGA* filler, and an increase in ρ_{dn} did not necessarily indicate the evolution of mechanical properties during compaction. Hence, in this study, the mechanical indicators K_{rb} and K_{20} were employed to characterize the mechanical properties of the *HRGA* filler during compaction.

Moreover, the dynamic characteristics of the vibration compactor conformed to the two-degree-of-freedom dynamic model, as shown in Figure 3(a). The motion equation of the vibration system is presented in Eq. (3).

$$m_d\ddot{x}_2+F_s=F+K_1(x_2-x_1)+C_1\left(\dot{x}_2-\dot{x}_1\right)+m_pg \tag{3}$$

where m_d is the mass of the vibration system, F_s is the contact force between the vibration system and *HRGA* filler, F is the vibration force, K_1 is the stiffness coefficient between the weight block and vibration system, x_2 is the vibration system displacement, x_1 is the weight block displacement, C_1 is the damping coefficient between the weight block and vibration system and m_p is the mass of the weight block.

According to the findings of Xie *et al.* (2023a, b), *HRGA* was classified as a viscoelastic material with damping, which results in a hysteresis effect between the *HRGA* filler displacement and the vibration force, as shown in Figure 3(b). Hence, it was necessary to consider the effect of the lag phase angle in the *HRGA* filler stiffness calculation, and the lag phase angle $\Delta\varphi$ could be calculated as follows:

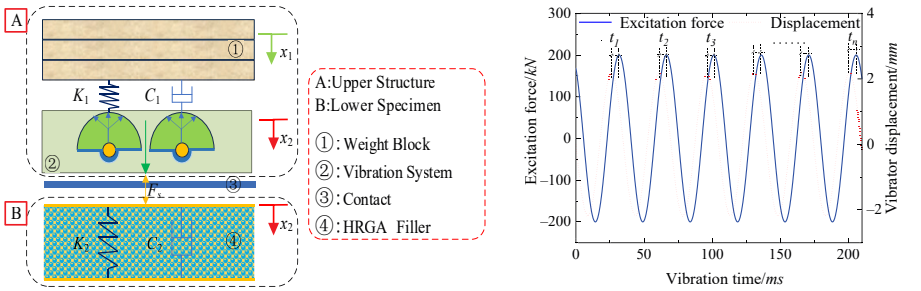

Figure 3. K_{rb} calculation graphic: (a) two-degree-of-freedom dynamic model and (b) lag phase angle Δφ calculation graphic. **Source(s):** Authors' own work

$$\Delta\varphi = \frac{\sum_{i=1}^{k} \Delta t_i}{k} \cdot v \tag{4}$$

where k is the number of periods of displacement in one sampling period, Δt_i is the i th time difference within a sampling period and v is the rotation speed of the eccentric block.

According to the previous research (Xie *et al.*, 2023a, b), the modified K_{rb} of *HRGA* filler could be calculated as follows:

$$K_{rb} = \frac{m_e r_e \omega^2 \sin(\Delta\varphi) + m_p g - m_d \ddot{x}_2|_{\dot{x}_2=0}}{x_2|_{\dot{x}_2=0}} \tag{5}$$

Additionally, the modulus of subgrade reaction (K_{30}) characterized the *HRGA* material's resistance to deformation and was employed to assess field compaction quality (China Railway First Survey and Design Institute Group Corporation Limited, 2010). It was measured using the field load test and could be calculated as follows:

$$K_{30} = \sigma_{1.25}/S_{1.25} \tag{6}$$

where $S_{1.25}$ represents a sinkage of 1.25 mm and $\sigma_{1.25}$ represents the load strength corresponding to a sinkage of 1.25 mm.

Similarly, the indoor load test could assess the bearing capacity of *HRGA* specimens during compaction. The diameter of the indoor load plate was 200 mm, while the diameter of the field load plate was 300 mm. To ensure that the indicator K_{20} corresponded to the K_{30}, which should comply with the similarity theory. According to the previous research, the indoor load test indicator K_{20} could be calculated as follows:

$$K_{20} = \sigma_{0.84}/S_{0.84} \tag{7}$$

where $S_{0.84}$ represents a sinkage of 0.84 mm and $\sigma_{0.84}$ represents the load strength corresponding to a sinkage of 0.84 mm.

The parameters $S_{0.84}$ and $\sigma_{0.84}$ of K_{20} could be measured by the indoor load test equipment (*IL-1*), which mainly consists of a jack, force ring and micrometer, as shown in Figure 4.

2.2.2 Novel vibration compactor. Building upon the findings of the above research, a conventional plate vibration compactor was optimized and a novel vibration compactor *IC-1* was designed. It mainly consisted an outer frame, lifting device, vibration equipment,

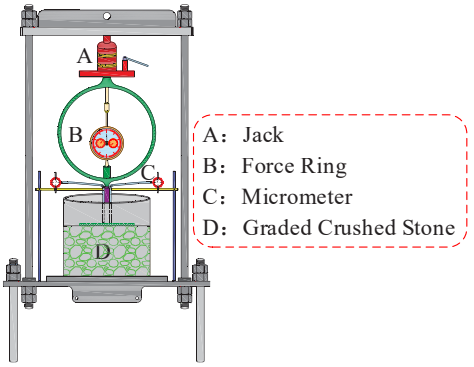

Figure 4. Indoor load test equipment IL-1. **Source(s):** Authors' own work

baseplate, displacement sensor, Hall sensor, accelerometer and intelligent control module, as shown in Figure 5, with the relevant parameters listed in Table 1. By applying the continuous dry density calculation equation (Eq. (2)), the ρ_d could be output in real-time using data from the displacement sensor. Similarly, by applying the modified dynamic stiffness calculation equation (Eq. (5)), the K_{rb} could be output in real-time using data from the acceleration sensor and Hall sensor.

2.3 Validation

To validate the accuracy of the novel vibration compactor and indoor load test equipment, the *HRGA* filler from Guangzhou-Zhanjiang High-speed Railway was prepared according to the *Code for Design of Railway Earth Structure (TB 10001–2016)* (National Railway Administration of the People's Republic of China, 2016), as shown in Figure 6. The *HRGA* filler settlement stabilized after seven continuous uniform passes by the roller compactor equipped with an accelerometer. The *HRGA* filler K_{rb} was measured through the accelerometer, and the K_{30} was measured at several locations within the test site through

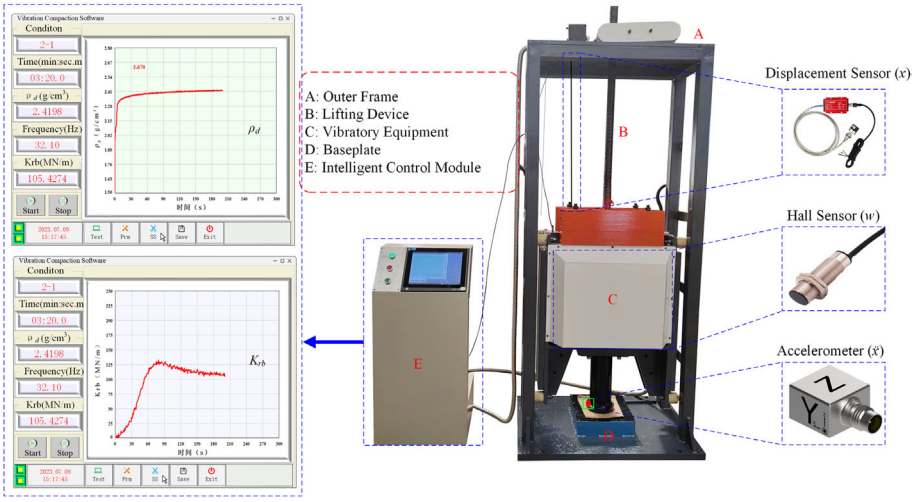

Figure 5. Vibration compactor IC-1. **Source(s):** Authors' own work

Table 1. IC-1 parameters

Serial number	Item	Specification
1	Dimensions (L*W*H)	800mm*1200mm*2000mm
2	Infinitely adjustable vibration frequency	0-80Hz
3	Maximum vibration mass	600kg
4	Minimum vibration mass	200kg
5	Exciting vibration mode	Biaxial counter-rotation
6	Eccentric block mass	4.7kg
7	Eccentric distance	0-5cm
8	Power	5kW

Source(s): Authors' own work

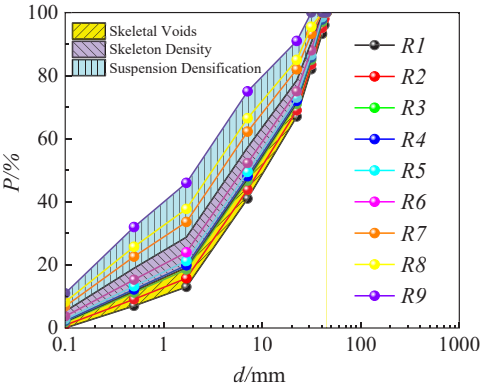

Figure 6. HRGA filler particle size distribution. **Source(s):** Authors' own work

plate load tests. Meanwhile, *HRGA* fillers from groups R1 to R9 were selected for the *IVCT* and indoor load tests as a comparison.

The *HRGA* filler K_{rb} and K_{30} test results are shown in Figure 8. The range for K_{rb} obtained in field tests was 132-195MN·m^{-1}, and in indoor tests was 150-174MN·m^{-1}. The range for K_{30} obtained in field tests was 190-245MPa·m^{-1}, and in indoor tests was 200-240MN·m^{-1}. It is important to note that the difference between the values obtained in indoor and field tests for K_{rb} and K_{30} was minimal. Hence, the novel vibration compactor and the indoor load test equipment were reliable mechanical indicators; K_{rb} and K_{30} could indicate the evolution of the *HRGA* filler's mechanical properties during compaction. Furthermore, the novel *IVCT* method could control the compaction quality of *HRGA* more effectively.

3. Materials and testing

3.1 Materials

The *HRGA* fillers used in *IVCT* were obtained from the Guangzhou-Zhanjiang High-Speed Railway. Three types of *HRGA* fillers were prepared in the laboratory, including skeleton voids gradation (*R1*), skeleton density gradation (*R2*) and suspension densification gradation (*R3*), as shown in Figure 6. Moreover, the same *HRGA* fillers were continuously rolled using the roller compactor until settlement stabilized in the field test, as shown in Figure 7. It was important to note that the ρ_{df} of R1, R2 and R3 was measured using the sand cone method with 2.11, 2.38 and 2.29 g·cm^{-3}.

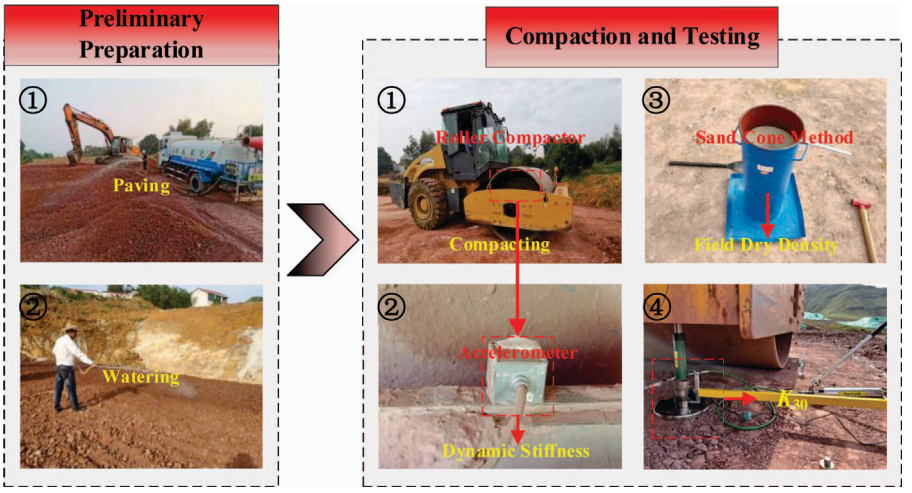

Figure 7. K_{rb} and K_{30} tests in the field. **Source(s):** Authors' own work

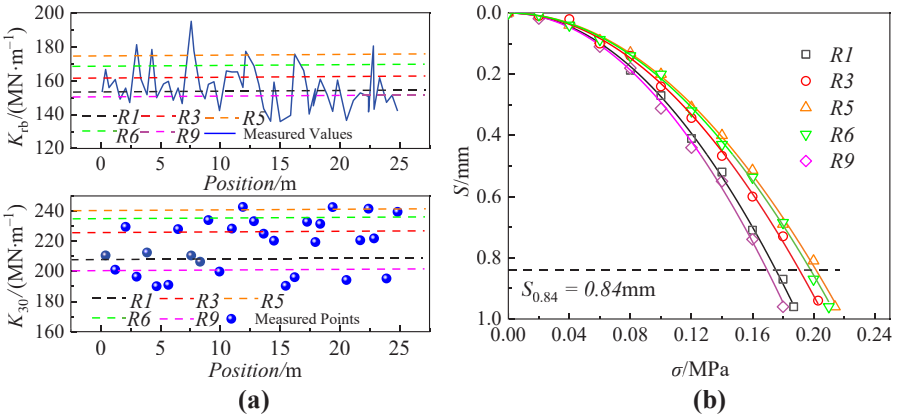

Figure 8. Mechanical indicators indoor-field results compared: (a) K_{rb} and K_{30} indoor-field compared and (b) K_{20} calculation process. **Source(s):** Authors' own work

3.2 Test design

Based on the control variable method, the optimal compaction parameters of the above *HRGA* fillers in *IVCT* were explored, including the optimal moisture content (ω_{opt}), the optimal container size (R_d and R_h) and the optimal vibration parameters (f, M_c and r_e). The main steps of the test were as follows:

(1) Specimen preparation: The *HRGA* fillers with different ω were prepared (*2%, 4%, 5%* and *6%)* and then left overnight to fully wet.

(2) Sample preparation: The HRGA filler (M_0 kg) was slowly poured into the container (D mm in diameter) and the surface was subsequently smoothed.

(3) Parameters configuration: The container was mounted on the vibration compactor and the vibration parameters (f, M_c, r_e and T) were set to conduct the test.

(4) Data acquisition: Based on the novel vibration compactor, the curves of ρ_d-t and K_{rb}-t were output in real-time by measuring S_n with displacement sensors, $\ddot{x}_2$ with acceleration sensors and F with Hall sensors.

4. Results analysis

4.1 Optimal ω

As was well known, ω_{opt} for *HRGA* fillers in traditional *IVCT* was determined using the heavy hammer compaction method (*HHCM*). Taking R2 as an example, the ω_{opt} was determined to be 4.4% by the *HHCM*, as shown in Figure 9(a). Then, the novel *IVCT* was conducted with the ω_{opt} of 4.4% for R2. It was important to note that serious defects occurred in R2 during compaction, including mud pumping at the vibration hammer and container base, scaling on the surface of *HRGA* fillers, and difficulties in forming, as shown in Figure 9(b). Hence, using *HHCM* to determine the ω_{opt} for *HRGA* fillers in the novel *IVCT* was inappropriate, and a new method to determine the ω_{opt} needs to be proposed.

Firstly, the novel *IVCT* was conducted with different ω for R2, and the curves of ρ_d-*t* were shown in Figure 10(a). It was found that the ρ_d increased rapidly in the early stages of compaction and then stabilized. Moreover, the ρ_{dmax} at different ω first decreased and then increased as ω increased, which differed from the trend observed in the *HHCM*. In addition, when the ω was lower (e.g., ω = 2%), defects were observed on the surface of *HRGA* fillers after demolding, and when the ω was greater (e.g., ω = 6%), mud pumping occurred during compaction, with difficulties in forming after demolding, as shown in Figure 10(b). It was important to note that when the ω was 4%, no mud pumping occurred during compaction, and the *HRGA* fillers were formed well after demolding.

Then, the ω before and after compaction was determined using the drying method, where the specimens were dried in an oven, as shown in Figure 10(c). It was found that when the initial ω was below 4%, it remained nearly unchanged after compaction. Nevertheless, when the initial ω was above 4%, water loss was caused by mud pumping during compaction, and the ω was stabilized at 4% after compaction. Hence, this stable ω could be selected as the ω_{opt} for *HRGA* fillers in the novel *IVCT*, which was referred to as the critical moisture content (*CMC*).

Finally, the novel *IVCT* was conducted with different ω for R1 and R3. It was important to note that the trends observed in R1 and R3 were consistent with R2. The ρ_{dmax} of R1 and R3 first decreased and then increased as ω increased and exhibited a "trough" trend, as shown in Figure 10(d). From Figure 10(e), the *CMC* values of R1, R2 and R3 were 3.6%, 4.0% and 5.4%, respectively. The *CMC* of R1, R2 and R3 was used as the ω_{opt} in the novel *IVCT*, and no

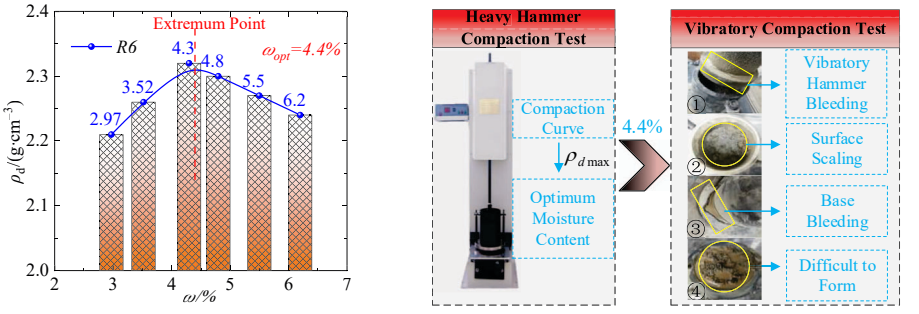

Figure 9. The defects of the *HHCM* to determine the ω_{opt} in the novel IVCT: (a) compaction curve of R2 and (b) defects in the novel *IVCT*. **Source(s):** Authors' own work

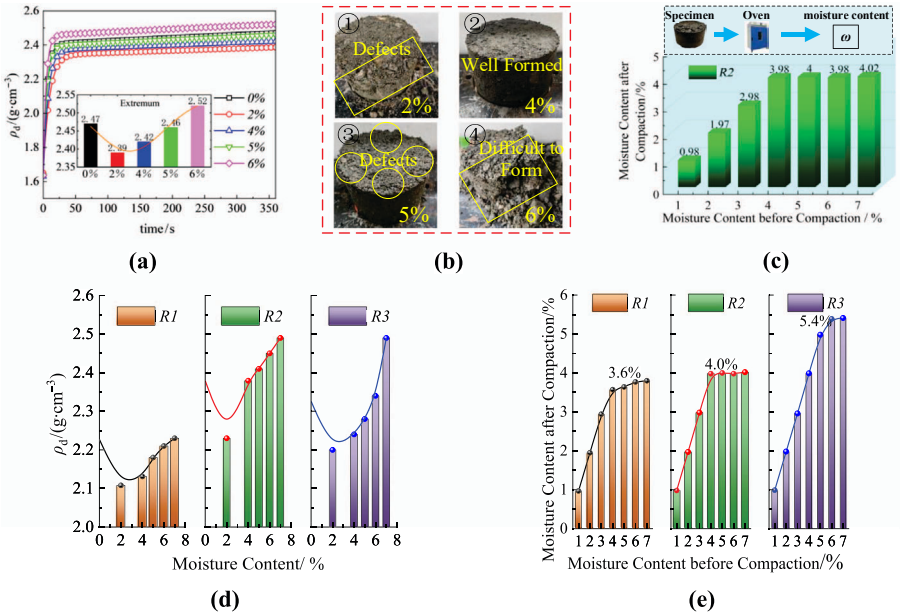

Figure 10. Physical properties of the novel *IVCT* with different ω: (a) the curves of ρ_d−t for R2, (b) R2 specimens after demolding, (c) the ω of R2 before and after compaction, (d) the effect of ω on the ρ_d and (e) the effect of compaction on the ω. **Source(s):** Authors' own work

mud pumping occurred during compaction. Moreover, taking R2 as an example, the ρ_d was measured as 2.38 g·cm^{-3} with the sand cone method in the field, while the ρ_{dmax} was 2.32 g·cm^{-3} using the *HHCM*, indicating the $K > 1$, which did not meet the specification requirements. The ρ_{dmax} measured at *CMC* in the novel *IVCT* was 2.42 g·cm^{-3}, and the $K = 0.983$, which met the specification requirements.

On the other hand, Figure 11(a) presented the evolution of K_{rb} for R2 at different ω. It was found that K_{rb} increased rapidly in the early stages of compaction and then gradually decreased. For different ω, K_{rb} reached its maximum value at different compaction time points, which could be selected as the optimal compaction time (T_{1p}). Moreover, if the t exceeded T_{1p}, K_{rb} tended to decrease. It was important to note that the maximum value of K_{rb} for R2 at *CMC* was higher than other ω. Similarly, K_{20} reached its maximum value at *CMC*, as shown in Figure 11(b). In addition, both K_{rb} and K_{20} of R1 and R3 at *CMC* reached their maximum values, as shown in Figure 11(c). Therefore, the physical-mechanical properties of *HRGA* fillers at *CMC* were optimal, suggesting that *CMC* could be selected as the ω_{opt} for *HRGA* fillers in the novel *IVCT*.

4.2 Optimal container size

To improve the compaction quality control for *HRGA* fillers, minimizing the size effect of the container in the *IVCT* was essential. This included optimizing the ratios: the container diameter (D) to the maximum particle size in *HRGA* fillers (referred to as R_d) and the initial fillers' thickness (H_0) to the maximum particle size (referred to as R_h). In this study, the optimal container size was determined using the novel *IVCT* by evaluating the physical-mechanical properties of different R_d and R_h ratios for R1, R2, R3 and R4 (uniform gradation *HRGA* fillers). The ω of R1, R2, R3 and R4 was set to *CMC*, the M_0 of specimens was 7.5kg and the vibration parameters were $M_c = 600$kg, $r_e = 2.5$cm and $f = 34$Hz.

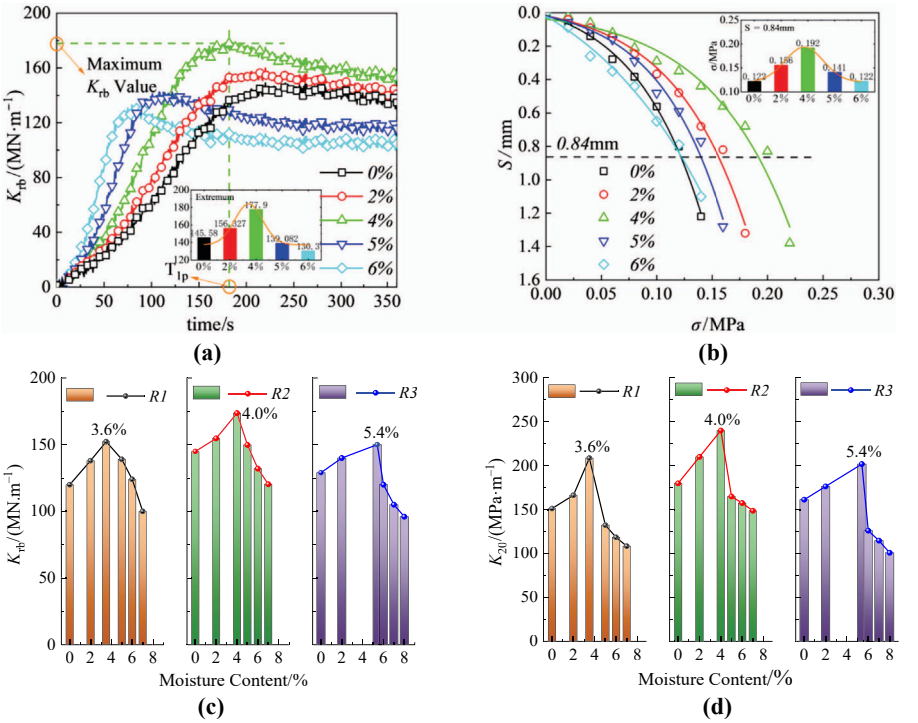

Figure 11. Mechanical properties of the novel *IVCT* with different ω: (a) the curves of K_{rb}-t for R2, (b) the load-settlement curves of R2, (c) the effect of ω on the K_{rb} and (d) the effect of ω on the K_{20}. **Source(s):** Authors' own work

4.2.1 Optimal R_d. The novel *IVCT* was conducted with various D (D = 100, 150, 200, 250 and 300mm) for R1, R2, R3 and R4, as shown in Figure 12. Figure 13 demonstrated the physical properties of R1, R2, R3 and R4 at different D. The evolution of ρ_d for R2 during compaction was presented in Figure 13(a), where ρ_d increased rapidly in the early stages of compaction and then stabilized. Moreover, the ρ_{dmax} initially increased with D and remained nearly unchanged when $D \geq$ 150mm. Furthermore, the evolution characteristics of the physical properties for R1, R3 and R4 were consistent with R2, as shown in Figure 13(b). Additionally, determining the representative particle size of *HRGA* fillers was crucial for achieving the optimal R_d. Due to the difficulty in determining the representative particle sizes of R1, R2 and R3, the maximum

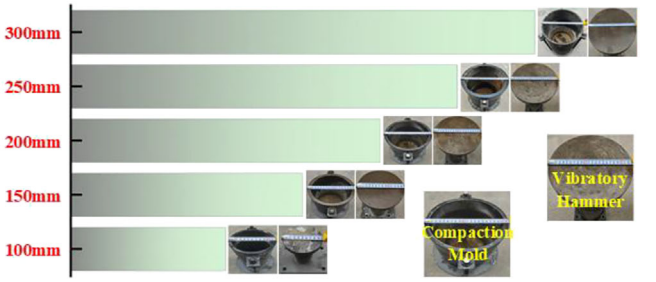

Figure 12. Containers with different D. **Source(s):** Authors' own work

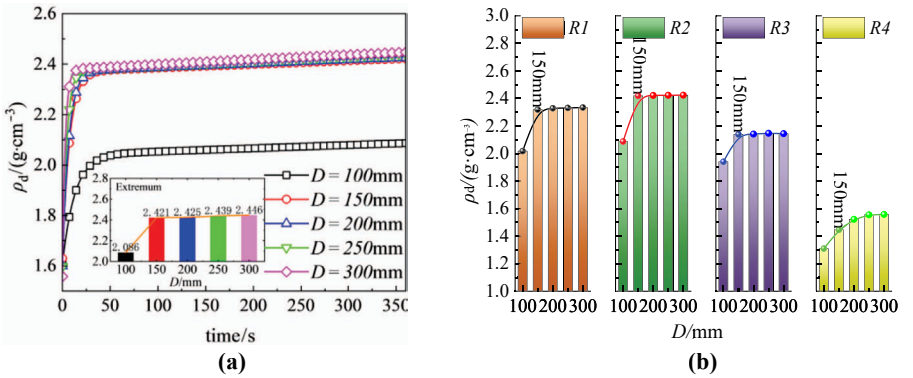

Figure 13. Physical properties of the novel *IVCT* with different *D* for *HRGA* fillers: (a) the curves of ρ_d-*t* for R2 and (b) the effect of *D* on the ρ_d. **Source(s):** Authors' own work

particle size (45mm) of R4 was selected as the representative particle size (d_e), whose ranges were from 31.5-45mm. It was important to note that when $D > 3.4d_e$, the increase in the physical properties of R4 became minimal. Hence, when $R_d(D/d_e) \geq 3.4$, the impact of *D* on the physical properties of *HRGA* fillers was minimal.

Figure 14 demonstrated the mechanical properties of R1, R2, R3 and R4 at different *D*. The evolution of K_{rb} for R2 during compaction was presented in Figure 14(a), where K_{rb} increased rapidly in the early stages of compaction and then gradually decreased. This trend suggested that the mechanical properties of *HRGA* fillers were optimized at T_{1p}. Moreover, the maximum K_{rb} initially increased with *D* and remained nearly unchanged when $D \geq 150$mm. Similarly, K_{20} remained stable at $D \geq 150$mm, as shown in Figure 14(b). Furthermore, the evolution characteristics of mechanical properties for R1, R3 and R4 were consistent with R2, as shown in Figure 14(c)-(d). It was important to note that when $D > 3.4d_e$, the increase in the mechanical properties of R4 became minimal. Hence, when $R_d(D/d_e) \geq 3.4$, the impact of *D* on the physical-mechanical properties of *HRGA* fillers was minimal, suggesting that 3.4 could be selected as the optimal R_d of the container for *HRGA* fillers in the novel *IVCT*.

4.2.2 Optimal R_h. The novel *IVCT* was conducted with different H_0 (H_0 = 120, 126, 138, 155, 188 and 205mm) for R1, R2, R3 and R4 as shown in Figure 15. Figure 16 demonstrated the physical properties of R1, R2, R3 and R4 with different H_0. The evolution of ρ_d for R2 during compaction was presented in Figure 16(a), where ρ_d increased rapidly in the early stages of compaction and then stabilized. Moreover, the ρ_{dmax} remained stable when $120 < H_0 < 155$ mm but rapidly decreased when $155 < H_0 < 205$ mm with the jump vibration of the hammer. Furthermore, the evolution trends of physical properties observed in R1, R3 and R4 were consistent with R2, as shown in Figure 16(b). Additionally, the representative particle size of *HRGA* fillers should be determined to obtain the optimal R_h. Due to the difficulty in determining the representative particle sizes of R1, R2 and R3, the maximum particle size (45mm) of R4 was selected as the representative particle size (d_e), whose ranges were from 31.5–45mm. It was important to note that the physical properties of R4 remained stable when $H_0 \leq 3.5d_e$ and rapidly decreased when $H_0 > 3.5d_e$. Hence, when $R_h(H_0/d_e) \leq 3.5$, the physical properties of *HRGA* fillers were optimal.

Figure 17 demonstrated the mechanical properties of R1, R2, R3 and R4 with different H_0. The evolution of K_{rb} for R2 during compaction was presented in Figure 17(a), where K_{rb} increased rapidly in the early stages of compaction and then gradually decreased. This trend suggested that the mechanical properties of *HRGA* fillers were optimized at T_{1p}. Moreover, the maximum K_{rb} increased and then decreased with H_0 and the maximum value was obtained at H_0 = 155mm. Similarly, K_{20} followed the same trend, as shown in Figure 17(b). Furthermore, the evolution trends of mechanical properties observed in R1, R3 and R4 were consistent with

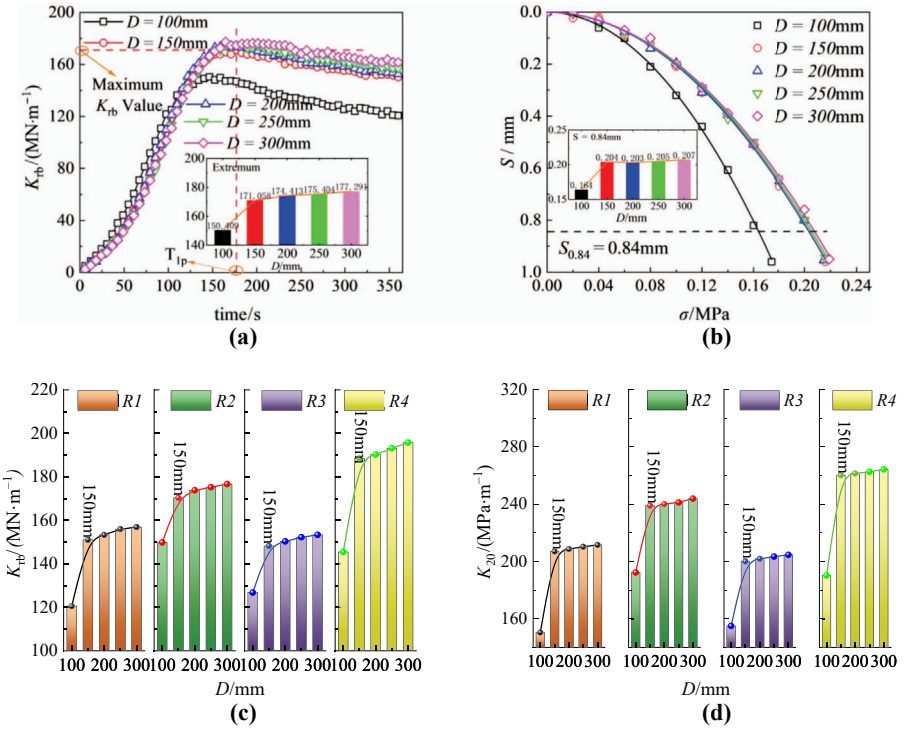

Figure 14. Mechanical properties of the novel IVCT with different D for HRGA fillers: (a) the curves of K_{rb}−t for R2, (b) the load-settlement curves of R2, (c) the effect of D on the K_{rb} and (d) the effect of D on the K_{20}. **Source(s):** Authors' own work

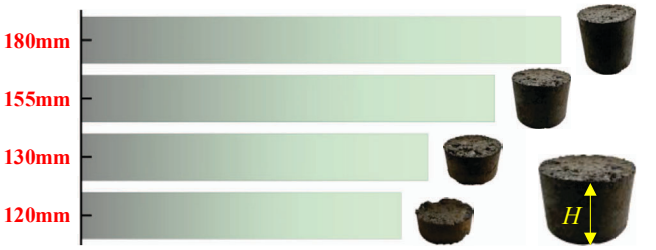

Figure 15. Initial HRGA fillers thickness (H0). **Source(s):** Authors' own work

R2, as shown in Figure 14(c)–(d). It was found that when $H_0 = 205$mm, the hammer occurred jump vibration; when H_0 was smaller, the *HRGA* fillers could be crushed seriously, and when $H_0 = 155$mm, the *HRGA* fillers could be abraded, as shown in Figure 14(e). It was important to note that when $H_0 = 3.5d_e$, the mechanical properties of R4 were optimal. Hence, when $R_h(H_0/d_e) = 3.5$, the physical-mechanical properties of *HRGA* fillers were optimal, suggesting that 3.5 could be selected as the optimal R_h for *HRGA* fillers in the novel *IVCT*.

4.3 Optimal vibration parameters

To improve the compaction quality control of *HRGA* fillers, the vibration parameters (f, M_c, and r_e) of the novel vibration compactor should be selected reasonably. Hence, based on the

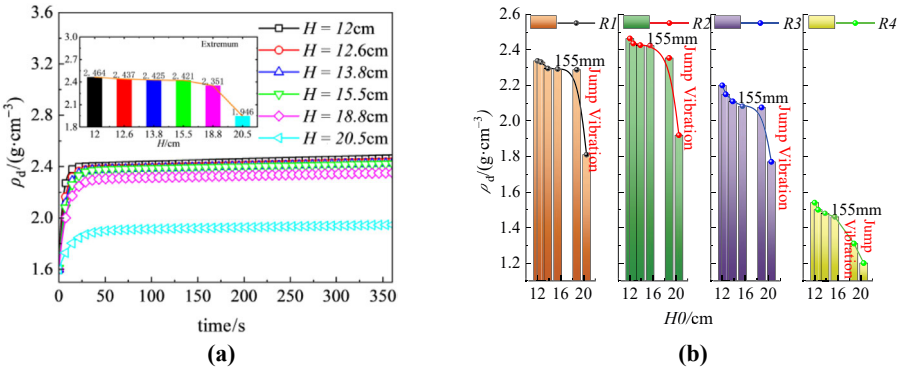

Figure 16. Physical properties of the novel *IVCT* with different *D* for *HRGA* fillers: (a) the curves of ρ_d-*t* for R2 and (b) the effect of H_0 on the ρ_d. **Source(s):** Authors' own work

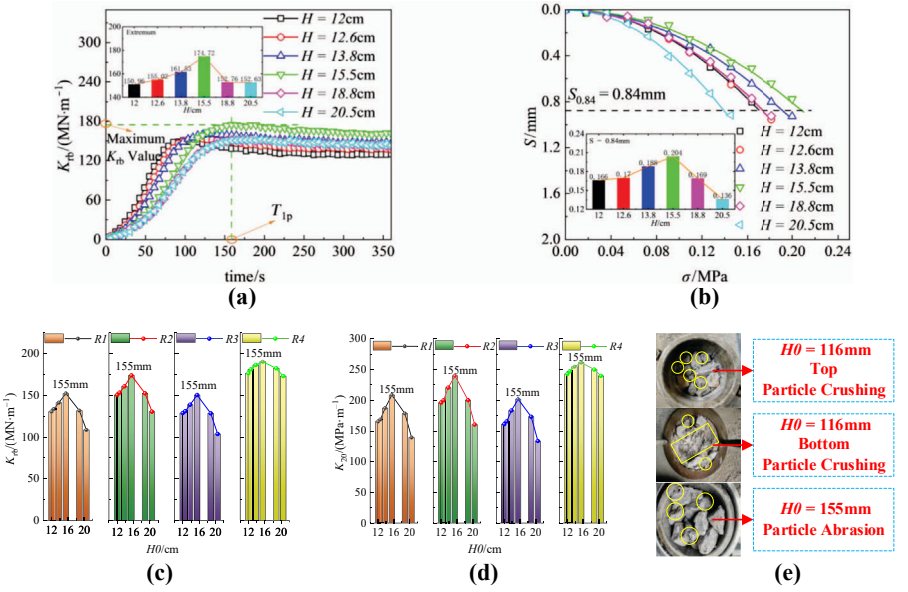

Figure 17. Mechanical properties of the novel IVCT with different H_0 for HRGA fillers: (a) the curves of K_{rb}-t for R2, (b) the load-settlement curves of R2, (c) the effect of H_0 on the K_{rb}, (d) the effect of H_0 on the K_{20} and (e) HRGA fillers crushing at different H_0. **Source(s):** Authors' own work

control variable method, the novel *IVCT* was conducted to determine the optimal vibration parameters through the physical-mechanical properties evolution of *HRGA* fillers. In addition, the other test parameters (ω, r_d and r_h) were set to the optimal parameters in 4.1 and 4.2.

4.3.1 Optimal f. According to previous research (Zhang, Liu, Zhang, & Huangfu, 2019; Li, Zho, & Li, 2012), the compaction system was at the resonance state when *f* approached the natural frequency (f_0) of the filler, which could lead to optimal physical-mechanical properties in fillers. As shown in Figure 18(a), the f_0 of *HRGA* fillers was determined using the hammer modal analysis method (HMAM) based on the research by Xiao *et al.* (2024a). The hammering modal analysis method consisted of four steps: specimen demolding, sensor installation, acceleration signal acquisition and signal analysis. It was important to convert the acceleration

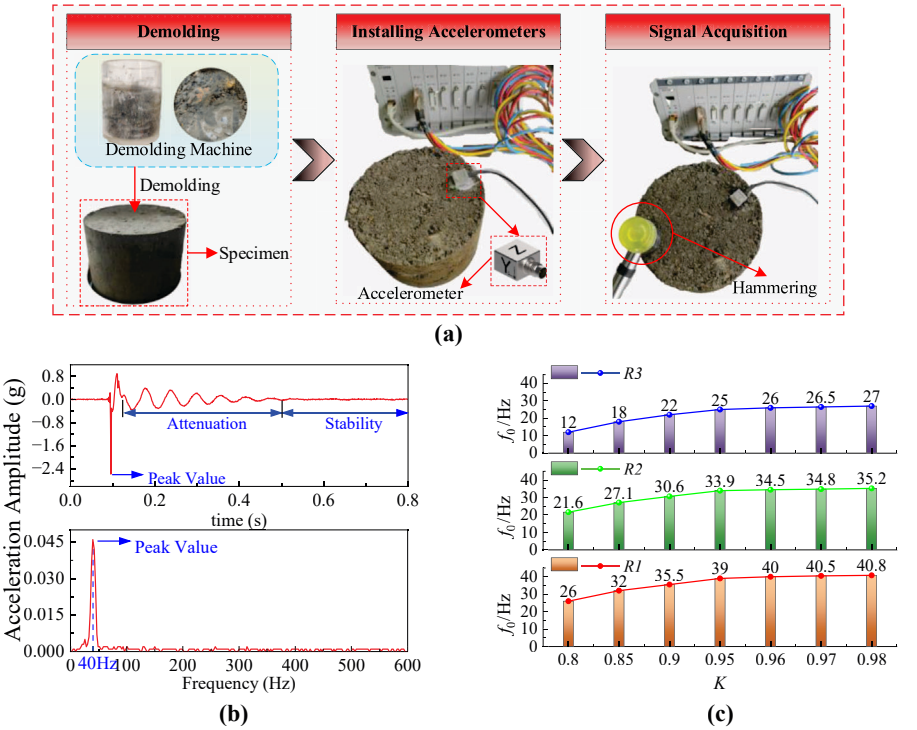

Figure 18. The process of determining f_0 for *HRGA* fillers: (a) *HMAM* test process, (b) *HMAM* analysis process for R2 and (c) the evolution of f_0 with K for R1, R2, and R3. **Source(s):** Authors' own work

signal into a spectral signal and then determine the filler's f_0 based on the peak of the spectral signal. Hence, the f_0 of R1, R2 and R3 was determined as 40Hz, 34Hz and 26Hz, respectively. Furthermore, as shown in Figure 18(b), it was found that the f_0 showed a trend of "rapid increase-slow increase" as K increased.

To validate the above, f_0 was the optimal vibration frequency (f_{op}) of the *HRGA* filler; taking R2 as an example, the novel *IVCT* was conducted at various f (f = 20, 24, 28, 32, 34, 36 and 40Hz). Figure 19 demonstrated the physical properties of R2 under different f. As shown in Figure 19(a), ρ_d increased rapidly in the early stages of compaction and then stabilized. Moreover, ρ_{dmax} initially increased and then gradually decreased with f increased, and the maximum value was obtained at f = 34Hz. Additionally, as shown in Figure 19(b) and (c), it was found that the physical properties initially increased and then gradually decreased with f increased under different M_c and r_e conditions when the compaction system was in a non-jumped vibration state. However, this trend was not observed under jump vibration. It was important to note that the physical properties of the *HRGA* fillers were optimal when $f = f_0$.

Figure 20 demonstrated the mechanical properties of R2 under different f. As shown in Figure 20(a), K_{rb} increased rapidly in the early stages of compaction and then gradually decreased, and the mechanical properties of *HRGA* fillers were optimized at T_{1p}. Moreover, the maximum K_{rb} initially increased and then gradually decreased with f increased, and the maximum value was obtained at f = 34Hz. Similarly, as shown in Figure 20(b), K_{20} followed the same trend. Additionally, as shown in Figure 20(c)-(f), it was found that the mechanical properties initially increased and then gradually decreased with f increased under different M_c and r_e conditions when the compaction system was in a non-jump vibration state. However, this trend was not observed under jump vibration. It was important to note that the mechanical

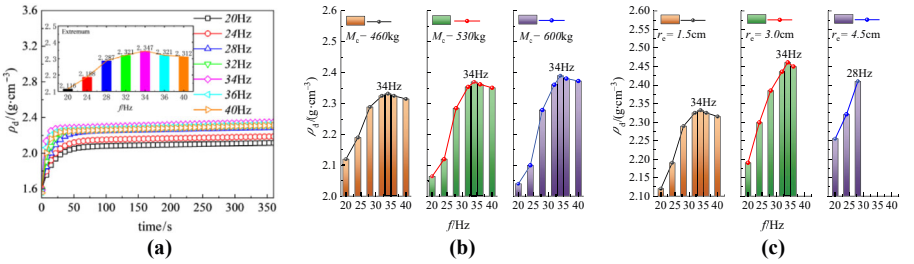

Figure 19. Physical properties of the novel *IVCT* with different *f* for HRGA fillers: (a) the curves of ρ_d-*t* for R2, (b) the effect of f on the ρ_d at different M_c and (c) the effect of f on the ρ_d at different r_e. **Source(s):** Authors' own work

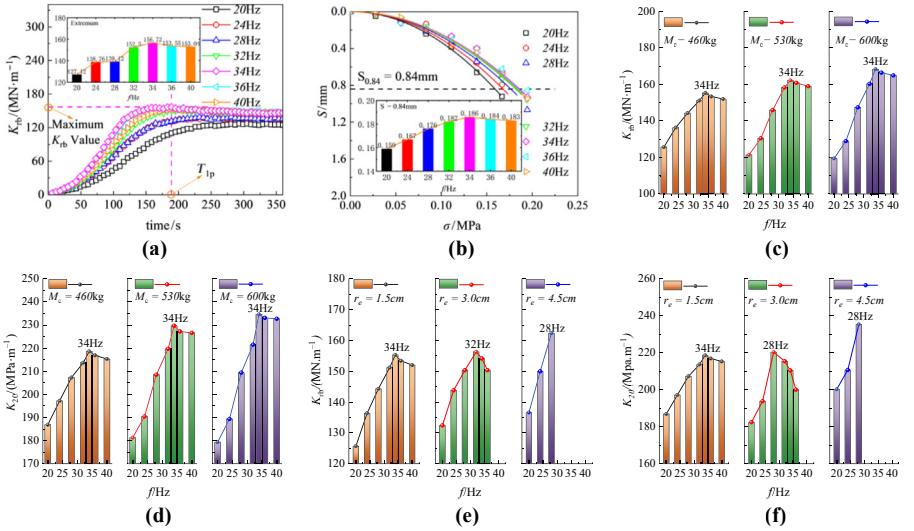

Figure 20. Mechanical properties of the novel IVCT with different f for HRGA fillers: (a) the curves of K_{rb}-t for R2, (b) the load-settlement curves of R2, (c) the effect of f on the K_{rb} at different M_c, (d) the effect of f on the K_{20} at different M_c, (e) the effect of f on the K_{rb} at different r_e and (f) the effect of f on the K_{20} at different r_e. **Source (s):** Authors' own work

properties of the *HRGA* fillers were optimal when $f = f_0$. Hence, suggesting that f_0 could be selected as f_{op} for *HRGA* fillers in the novel *IVCT*.

4.3.2 Optimal M_c. The novel *IVCT* was conducted at various M_c (M_c = 360, 460, 488, 516, 544, 572 and 600kg). Figure 21 demonstrated the physical properties of R2 under different M_c (f = 34Hz). As shown in Figure 21(a), ρ_d increased rapidly in the early stages of compaction and then stabilized. Moreover, ρ_{dmax} initially increased, then decreased, and stabilized when $M_c \geq$ 560kg, as M_c increased. Additionally, as shown in Figure 21(b), the physical properties continuously increased with M_c increased, the rate of increase gradually decreased; when r_e = 1.5cm or 4.5cm. The physical properties initially increased, then decreased and eventually stabilized when r_e = 3.0cm. Notably, the compaction system was in a jump vibration state when re = 4.5cm and re = 3.0cm with Mc < 560kg. The compaction system was in a resonance state when re = 3.0cm with Mc > 560kg. It was important to note that the ratio of the excitation force (F) to the vibration static load ($9.8M_c$) was 1.8 under the "resonance stabilization" state. Hence, the physical properties of *HRGA* fillers were optimal when the ratio of F to $9.8M_c$ was 1.8.

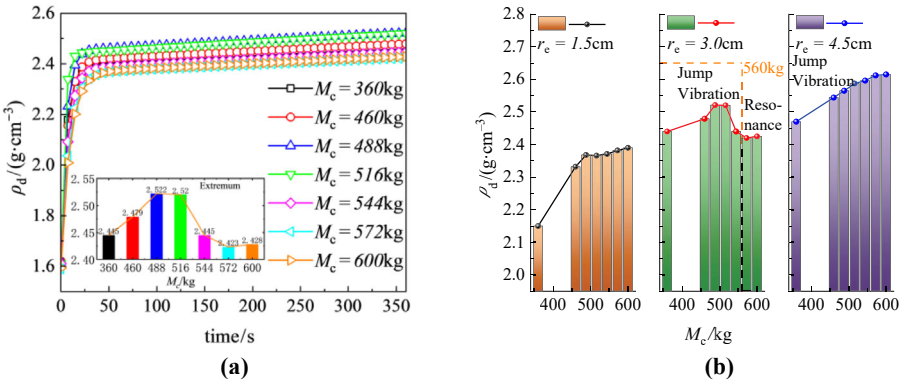

Figure 21. Physical properties of the novel IVCT with different M_c for HRGA fillers: (a) the curves of ρ_d-t for R2 and (b) the effect of M_c on the ρ_d at different r_e. **Source(s):** Authors' own work

$$F = 8\pi^2 m_e r_e f^2 \tag{8}$$

Figure 22 demonstrated the mechanical properties of R2 under different M_c(f = 34Hz). As shown in Figure 22(a), K_{rb} increased rapidly in the early stages of compaction and then gradually decreased, and the mechanical properties of *HRGA* fillers were optimized at T_{1p}.

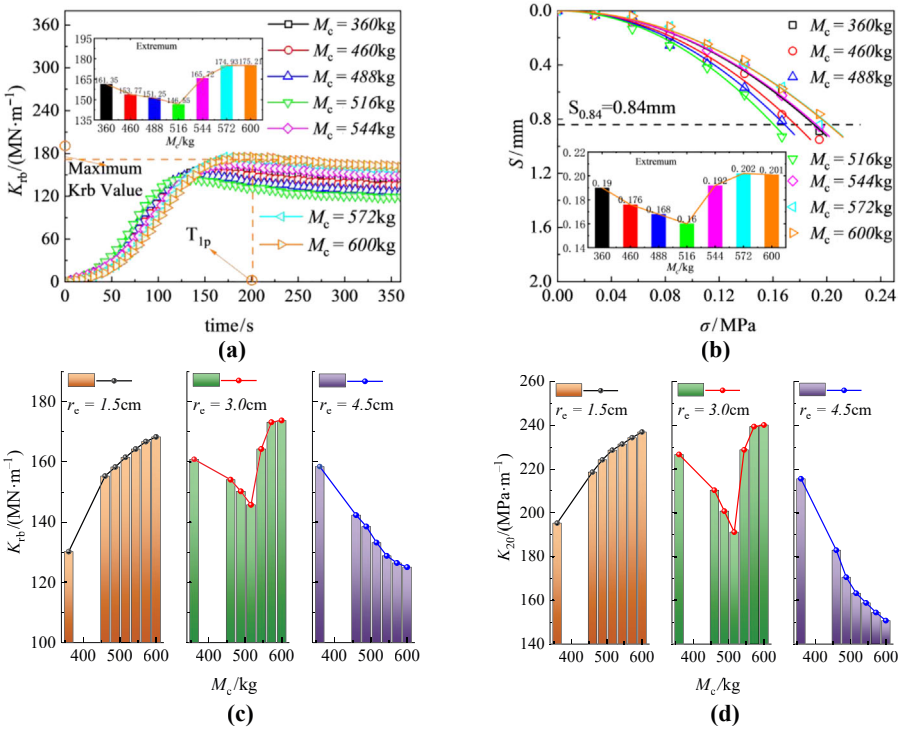

Figure 22. Mechanical properties of the novel IVCT with different M_c for HRGA fillers: (a) the curves of K_{rb}-t for R2, (b) the load-settlement curves of R2, (c) the effect of M_c on the K_{rb} at different r_e and (d) the effect of M_c on the K_{20} at different r_e. **Source(s):** Authors' own work

Moreover, the maximum K_{rb} initially decreased, then increased and stabilized when $M_c \geq 560$kg, as M_c increased. Similarly, as shown in Figure 22(b), K_{20} followed the same trend. Additionally, as shown in Figure 22(c) and (d), the evolution of mechanical properties with M_c presented different patterns under various r_e conditions. The mechanical properties continuously increased with M_c increased and the rate of increase gradually decreased when $r_e = 1.5$cm. Moreover, the compaction system was in a jump vibration state, and the mechanical properties continuously decreased with M_c increased when re = 4.5cm. Furthermore, the mechanical properties initially decreased, then increased and stabilized with M_c increased when $r_e = 3$cm. Notably, the compaction system was in a jump vibration state when $M_c < 560$kg and in a resonance state when $M_c > 560$kg. The mechanical properties of *HRGA* fillers were optimal under the "resonance stabilization" state, where the ratio of F to $9.8M_c$ was 1.8. Hence, the physical-mechanical properties of *HRGA* fillers in the novel *IVCT* were optimal when the ratio of F to $9.8M_c$ was 1.8.

4.3.3 Optimal r_e. The novel *IVCT* was conducted at various r_e (r_e = 1.5, 2.0, 2.5, 3.0 and 3.5cm). Figure 23 demonstrated the physical properties of R2 under different r_e ($M_c = 600$kg, $f = 34$Hz). As shown in Figure 23(a), ρ_d increased rapidly in the early stages of compaction and then stabilized. Moreover, ρ_{dmax} continuously increased with r_e increased; the compaction system occurred jump vibration when $r_e = 3.0$ and 3.5cm. Additionally, as shown in Figure 23 (b), the physical properties continuously increased with r_e increased, and the compaction system occurred jump vibration when the ratio of F to $9.8M_c$ exceeded 1.8. Hence, the physical properties of *HRGA* fillers were optimal when the ratio of F to $9.8M_c$ was 1.8.

As shown in Figure 24(a), K_{rb} increased rapidly in the early stages of compaction and then gradually decreased, and the mechanical properties of *HRGA* fillers were optimized at T_{1p}. Moreover, the maximum K_{rb} slowly increased as r_e increased and then rapidly decreased when re > 2.5cm. Similarly, as shown in Figure 24(b), K_{20} followed the same trend. Additionally, as shown in Figure 24(c) and (d), it was found that the mechanical properties slowly increased and then rapidly decreased with f increased under different M_c conditions. Notably, the mechanical properties of *HRGA* fillers were optimal when the ratio of F to $9.8M_c$ was 1.8. Hence, the physical-mechanical properties of *HRGA* fillers in the novel *IVCT* were optimal when the ratio of F to $9.8M_c$ was 1.8.

4.4 Parameters determination method

Based on the evolution in the physical-mechanical properties of *HRGA* fillers in the above novel *IVCT*, a method for determining the optimal compaction parameters had been proposed, as shown in Figure 25:

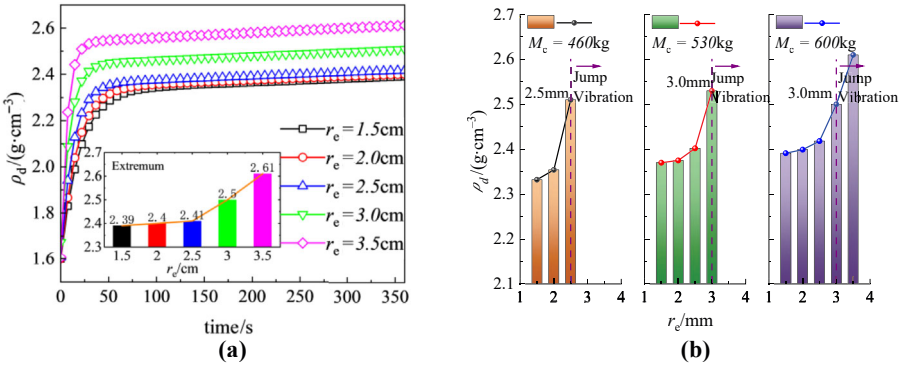

Figure 23. Physical properties of the novel IVCT with different r_e for HRGA fillers: (a) the curves of ρ_d-t for R2 and (b) the effect of r_e on the ρ_d at different M_c. **Source(s):** Authors' own work

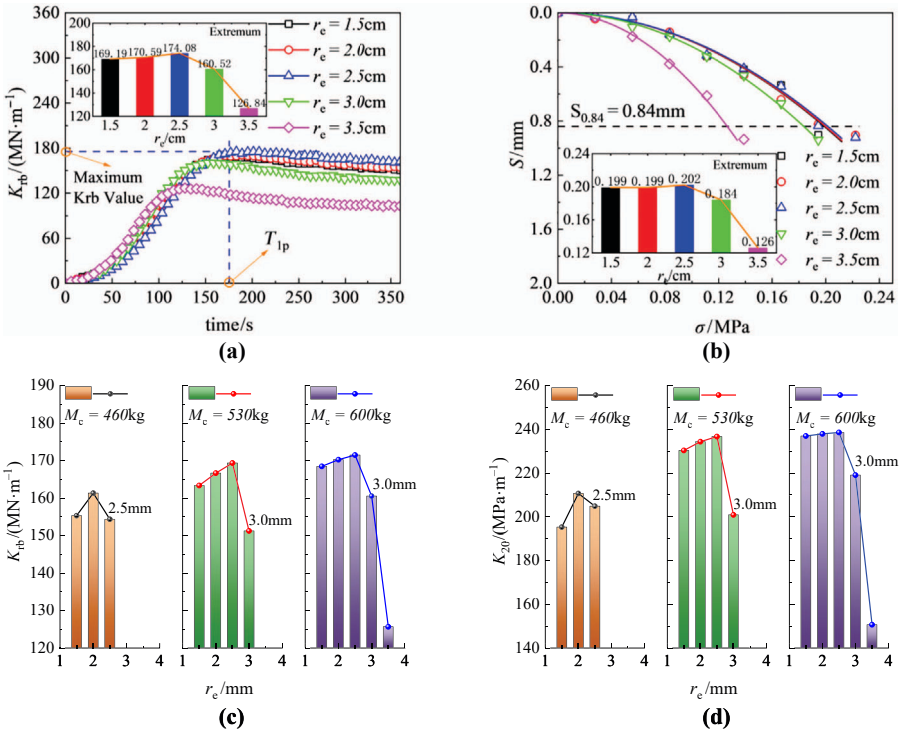

Figure 24. Mechanical properties of the novel IVCT with different r_e for HRGA fillers: (a) the curves of K_{rb}-t for R2, (b) the load-settlement curves of R2, (c) the effect of r_e on the K_{rb} at different M_c and (d) the effect of r_e on the K_{20} at different M_c. **Source(s):** Authors' own work

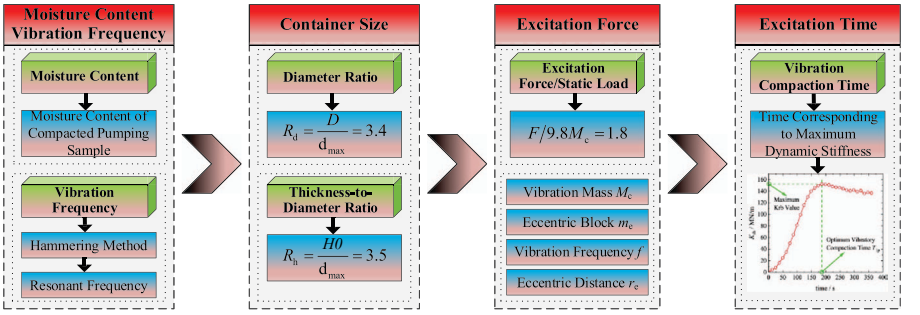

Figure 25. Method of determining parameters in the novel IVCT. **Source(s):** Authors' own work

(1) The ω_{opt} and f_{op} of *HRGA* fillers were obtained through calibration in laboratory tests;

(2) The optimal container dimensions were determined as R_d = 3.4 and R_h = 3.5 to minimize the size effect of the container in the novel *IVCT;*

(3) M_c and r_e were adjusted so that the ratio of F to 9.8M_c equaled 1.8, enabling the vibration compactor to achieve a resonance-stabilized state and

(4) T_{1p} was taken as the time corresponding to the "inflection point" on the K_{rb}-t curve.

5. Conclusions

Traditional IVCT had limited low applicability and reliability due to the one-sidedness of assessment indicators and uncertainty of compaction parameters. In this paper, a novel *IVCT* method was proposed based on multiple physical-mechanical indicators, including dry density (ρ_d), dynamic stiffness (K_{rb}) and bearing coefficient (K_{20}). Then, the optimal compaction parameters for the *IVCT*, including the optimal moisture content (ω), the optimal container size (e.g., R_d and R_h) and the optimal vibration parameters (e.g. f, M_c and r_e), were determined based on the evolution characteristics for multiple physical-mechanical indicators during compaction. The main conclusions were as follows:

(1) A continuous ρ_d calculation method, based on a surface settling model, had been proposed and validated. Similarly, a modified K_{rb} calculation method was proposed with the vibratory compaction dynamics model, and the accuracy of the improved vibratory compactor was also validated with field tests.

(2) During compaction, the ρ_d gradually increased with a decreasing rate. The K_{rb} initially increased and then decreased, with the inflection time T_{1p} identified as the optimal compaction time, indicating that the compaction time beyond T_{1p} would produce vibration degradation.

(3) Based on the evolution characteristics for multiple physical-mechanical indicators during compaction, the ω was determined as the water-holding content after mud pumping, with an optimal diameter-to-maximum particle size ratio (R_d) of 3.4 and an optimal thickness-to-maximum particle size ratio (R_h) of 3.5.

(4) The optimal vibration parameters were also determined, which was to control the ratio of the excitation force and the vibration mass (M_c) at 1.8, by taking the vibration frequency (f) as the resonance frequency and adjusting the vibration mass (M_c) and the eccentric distance (r_e).

References

Chawla, S., & Shahu, J. T. (2016). Reinforcement and mud-pumping benefits of geosynthetics in railway tracks: Numerical analysis. *Geotextiles and Geomembranes*, *44*(3), 344–357. doi: 10.1016/j.geotexmem.2016.01.006.

Chen, X. B., Xie, K., Li, T. F., & Zhang, Q. L. (2023). Investigation on the coarse-grained rearrangement of vibratory compaction in the high-speed railway graded aggregate materials. *Case Studies in Construction Materials*, *19*, e02385. doi: 10.1016/j.cscm.2023.e02385.

China Railway First Survey and Design Institute Group Corporation Limited (2010), Code for soil test of railway engineering, TB 10102-2010. China Railway Publishing house. (In Chinese).

Dan, H. C., Yang, D., Liu, X., Peng, A. P., & Zhang, Z. (2020). Experimental investigation on dynamic response of asphalt pavement using Smart Rock sensor under vibrating compaction loading. *Construction and Building Materials*, *247*, 118592. doi: 10.1016/j.conbuildmat.2020.118592.

Indraratna, M. B., & Nguyen, T. T. (2021). Experimental insights into the stiffness degradation of subgrade soils prone to mud pumping. *Transportation Geotechnics*, *27*, 100490. doi: 10.1016/j.trgeo.2020.100490.

Lan, C. H., Yang, Z., Liang, X. L., Yang, R., Li, P., Liu, Z., . . . Luo, W. (2023). Experimental study on wayside monitoring method of train dynamic load based on strain of ballastless track slab. *Construction and Building Materials*, *394*, 132084. doi: 10.1016/j.conbuildmat.2023.132084.

Li, J., Zhou, Z. L., & Li, Y. (2012). Test analysis of relationship between natural frequency and compaction degree for roadbed soil. *Transactions of the Chinese Society of Agricultural Engineering*, *28*, 71–76, (In Chinese).

National Railway Administration of the People's Republic of China (2016). *Code for Design of Railway Earth Structure*, TB10001-2016. Beijing: China Railway Publishing House.

Research Institute of Highway Ministry of Transport (2019). Field test methods of highway subgrade and pavement, JTG 3450-2019. People's Transport Publishing House, (In Chinese).

Sarsam, S. I., & Jumaah, M. K. (2016). Modeling of comparative performance of asphalt concrete under hammer, gyratory, and roller compaction. *Journal of Engineering*, *22*(11), 1–15. doi: 10.31026/j.eng.2016.11.01.

Spagnoli, G., & Shimobe, S. (2020). An overview on the compaction characteristics of soils by laboratory tests. *Engineering Geology*, *278*, 105830. doi: 10.1016/j.enggeo.2020.105830.

Wang, M., Yu, Q. D., & Xiao, Y. J. (2022). Experimental investigation of macro-and meso-scale compaction characteristics of unbound permeable base materials. *Chinese Journal of Rock Mechanics and Engineering*, *41*(8), 1701–1716. doi: 10.13722/j.cnki.jrme.2021.0912.

Wang, W. W., Li, C., Zhao, X. C., Song, P., Li, J., Zheng, J., & Wang, X. (2024). An Image-based method for evaluating changes in particle size and morphology distributions of aggregate materials after vibratory compaction test. *Construction and Building Materials*, *430*, 136483. doi: 10.1016/j.conbuildmat.2024.136483.

Wu, Y., Fu, H. R., & Bian, X. C. (2024). Comparative study on dynamic responses of ballasted and ballastless tracks at critical velocity. *Transportation Geotechnics*, *48*, 101354. doi: 10.1016/j.trgeo.2024.101354.

Xiao, X. P., Xie, K., Li, X. Z., Hao, Z. r., Li, T. F., & Deng, Z. X. (2023). Macro- and micro-deterioration mechanism of high-speed railway graded gravel filler during vibratory compaction. *Construction and Building Materials*, *409*, 134043. doi: 10.1016/j.conbuildmat.2023.134043.

Xiao, X. P., Li, T. F., Feng, L., Li, X., Hao, Z., & Li, J. (2024a). A framework for determining the optimal vibratory frequency of graded gravel fillers using hammering modal approach and ANN. *Sensors*, *24*(2), 689. doi: 10.3390/s24020689.

Xiao, X. P., Xie, K., Li, X. Z., Li, T. F., Deng, Z. X., Hao, Z. R., & Huang, Y. S. (2024b). Deterioration micro-mechanism of graded aggregates with different gradations under vibratory compaction using X-CT testing. *Measurement*, *235*, 114938. doi: 10.1016/j.measurement.2024.114938.

Xie, K., Chen, X. B., Li, T. F., Deng, Z. X., Yao, J. K., & Tang, L. B. (2023a). A framework for determining the optimal moisture content of high-speed railway-graded aggregate materials based on the lab vibration compaction method. *Construction and Building Materials*, *392*, 131764. doi: 10.1016/j.conbuildmat.2023.131764.

Xie, K., Chen, X. B., Li, T. F., Xiao, X. P., Tang, L. B., & Wang, Y.S. (2023b). Experimental and numerical study on the influence of deterioration on the mechanical properties of graded gravel fillers during vibratory compaction. *Construction and Building Materials*, *404*, 133153. doi: 10.1016/j.conbuildmat.2023.133153.

Yang, Z. H., Yue, Z. R., & Tai, B. (2021). Investigation of the deformation and strength properties of fouled graded macadam materials in heavy-haul railway subgrade beds. *Construction and Building Materials*, *273*(1), 121778. doi: 10.1016/j.conbuildmat.2020.121778.

Ye, Y. S., Cai, D. G., Yao, J. K., Wei, S., Yan, H., & Chen, F. (2021a). Review on the dynamic modulus of coarse-grained soil filling for high-speed railway subgrade. *Transportation Geotechnics*, *27*, 100421. doi: 10.1016/j.trgeo.2020.100421.

Ye, Y. S., Chen, X. B., & Hui, X. H. (2021b). Laboratory investigation on parameter optimization of vibrating compaction for high-speed railway's Group B. *Journal of Railway Science and Engineering*, *18*(10), 2497–2505. doi: 10.19713/j.cnki.43-1423/u.T20201127.

Yong, Y., Jiang, Y. J., Tian, T., Fan, J., Deng, C., & Xue, J. (2022). Mechanical-strength-growth law and predictive model for ultra-large size cement-stabilized macadam based on the vertical vibration compaction method. *Construction and Building Materials*, *324*, 126691. doi: 10.1016/j.conbuildmat.2022.126691.

Zhang, Q., Liu, T., Zhang, Z., & Huangfu, Z. (2019). Compaction quality assessment of rockfill materials using roller-integrated acoustic wave detection technique. *Automation in Construction*, *97*, 110–121. doi: 10.1016/j.autcon.2018.11.003.

Corresponding author
Ronghui Yan can be contacted at: rhyan206@163.com

Ronghui Yan worked as a visiting researcher in the University of Idaho. She is now an associate professor of Suzhou City University. Her research interests focus on infrastructure health monitoring for transportation, signal processing and pattern recognition.